Designing a 3D printable polypropylene-based material from after use recycled disposable masks

# Designing a 3D printable polypropylene-based material from after use recycled disposable masks.

D. Battegazzore*, F. Cravero, G. Bernagozzi, A. Frache

*Dipartimento di Scienza Applicata e Tecnologia*
*Politecnico di Torino, Alessandria Site, V.le Teresa Michel 5, 15121, Alessandria, Italy*

**Corresponding author.*
*Tel/Fax: +390131229343/+390131229399; e-mail address: daniele.battegazzore@polito.it*

## Abstract

Different percentages of talc were added to polypropylene deriving from pristine surgical masks in a small scale extrusion equipment to confer specific rheological and thermal properties to the resulting materials. This is not a fully satisfactory solution, thus the quantity of masks has been partially replaced by a first-use polypropylene copolymer. Two selected formulations with 35 and 50 wt.% of material deriving from pristine masks and 30 wt.% of talc have been identified as suitable for the 3D printing process.

Finally, the formulations were scaled up with a lab twin-screw extruder and by recycling sanitized after use masks to be as close as possible to field recycling conditions. The extruded pellets were processed to produce printing filament and finally validated as extrusion material for 3D printing. 3D printed tensile specimens were characterized for the mechanical properties and observed for their microstructure even comparing them with a commercial 3D printable material. For the first time is verified that a 3D printable extrusion material recycled from the disposable face masks can be obtained and shows comparable stiffness and strength to a commercial one.

*Keywords: Recycled PP; Face mask; 3D printing; Mechanical properties; Rheology.*

## 1. Introduction

The SARS-CoV-2 virus in 2020 caused the first pandemic of the twenty-first century, revolutionizing our daily habits. The most striking example is the adoption of facial masks as the main means for the infection reduction. In most cases, these Personal Protective Equipment "PPE" are made of polymeric material and disposable [1-3]. The environmental impact is therefore not negligible [4-11]. Muthu et al. have developed a model allowing the calculation of an environmental impact index (EI) for the production of fibres [12]. The higher the EI, the greater the negative impact on the environment.

Using the EI coefficient, Hartanto and Mayasari analysed a series of tissues used for the production of surgical and non-surgical masks [13]. In particular, fabrics made of polypropylene (PP) have the highest EI value, 34, in comparison to cotton (16), linen (12), wool (21) and even other synthetic fibres as polyester (30) [13]. In a 2021 published survey it was found that the majority of Italian citizens (> 70%) use surgical masks [14], namely those that give the highest EI index. In the same survey, 93% of respondents assert the willingness to collect the after use masks in a dedicated bin. This important propensity makes a strategic recycling program more likely to be designed, as a quantity of 600 g/year per capita is potentially generated, the 3% of the quantity of recyclable plastic material [14]. The treatment of such waste must then follow the procedure deriving from national legislation. In this research, both pristine masks from a single manufacturer and after use mask derived from dedicated bins collection in schools and companies were used. In these places new masks are delivered at the entrance and thrown after their use at the exit. The used PPE were sanitized according to current legislation by a specialized company using one of the methods also suggested in the literature [15-18].

It should be then emphasized that such kind of masks are made of micro-fibres, as the individual diameters are micrometric [19]. Accordingly, face masks are potential pollution source and are easily ingested by organisms in the aquatic life, affecting the food chain [5].

According to a study by Narita et al., the $CO_2$ emissions from the production of polypropylene would amount to 1.4 kg per kg of polymer [20]. The PP in every surgical mask is about 2 g, corresponding to approximately 3 g of $CO_2$. Moreover, based on a survey made in Italy [14], the use of 4 masks per person per week is likely to be a reasonable estimation. Thus, the monthly carbon footprint for the production of masks in Italy is calculated as $CO_2$ per mask ($3\times10^{-6}$ ton) × Italian population ($60\times10^{6}$) [21] × number of masks in a month (4×4) [14] = 2880 ton eq. $CO_2$. As an example, to produce the equivalent amount of $CO_2$, a vehicle emitting 120 g $CO_2$/km has to travel for 24 million km, or 600 times the circumference of the Earth.

The above calculation underestimates the real environmental impact (Life Cycle Assessment) because ignores the emissions due to transport of the manufactured product and its disposal. However, it helps to quantify the impact on the environment if the PP material is not recycled. Indeed, the reuse of PP from masks is able to partially reduce the $CO_2$ generation for the production of new PP for new objects.

A further problem was raised in recent studies that analysed the composition and recyclability of face masks [14, 19, 22]. In fact, masks are made of many materials which are hardly to be recycled

together, including metal. In particular, the filtering face part was shown to be made of PP in all the surgical masks analysed and only this part was used in this study [14, 19, 22]. Therefore, a selection and a shredding process was essential to effectively recover PP for recycling and resulting costs have to be considered.

On the other hand, PP is considered a "commodity", therefore its recycling must be encouraged and developed for high added value products where the profit margin allows economically sustainable recycling. One of the eligible sectors is certainly 3D printing extrusion technique also known as Fused Deposition Modeling (FDM) or Fused Filament Fabrication (FFF), where the price of the filaments is much higher than the price of the material itself. In particular, PP was previously studied in the literature as a technological solution and Bertolino et al. [23] have identified two main features for a PP-based material to be 3D printable.

In that study they found that the melting or crystallization enthalpy must be minimized and a strong shear thinning effect as well as a yield stress have to be present in the rheological curve. None of these prerequisites were identified in the neat material of the masks [19], therefore it must be modified. Following the work of Bertolino et al. [23] made on first use PP, the solution of adding talc as an inorganic filler, to confer the desired properties, was applied as a starting point in this study.

In another study by Jin et al. [24], further requirements have been highlighted for a PP in order to be 3D printable. Specifically, a PP copolymer is preferable along with the additions of additives to minimize the shrinkage. Following the suggestion of Jin et al. [24], a specific PP copolymer was selected and added to the masks material.

The ever-growing search for more sustainable materials also concerns additive manufacturing and focuses on the development of filaments from recycled material [25, 26]. A study by Zander et al. analysed the use of PET obtained from plastic containers for salads, PP from yogurt containers and PS from Petri dishes [27]. The aforementioned materials were extruded in the form of a dog bone specimen and tensile tested. Recycled PET had the highest tensile strength of 35±8 MPa while the neat rPP showed a strength of 20.1±2.3 MPa.

Pickering et al. used post-consumer recycled PP to fabricate a range of 3D printing filaments of 3 mm diameter. The mechanical testing on the filament showed tensile strength of 23.3 MPa and modulus of 1.02 GPa [28].

Vidakis et al. [29] analysed the mechanical response of Polypropylene over multiple recycling processes on 3D printed parts and they found a slight decrease (15%) in the tensile stress at break from 1st to 6th recycling course. Also Spoerk et al. [30] analysed the multiple recycling of PP with a

mineral filler and obtained minimal variations up to 15 cycles. These results are important because extends recycling to several times on the same PP material. Pan et al. characterized the recycled high-density polyethylene (HDPE)/PP 1.75 mm filament (r-PE PP) obtaining a yield strength of 13.6 MPa and a Young modulus of 1.23 GPa [31]. Morales et al. [32] presents the development and characterization of a 3D printing filament based on recycled PP. Mechanical tests showed high dependence of the mechanical properties on the 3D printing raster angle. Modulus values of 1.34 and 0.74 GPa and strength of 26 and 4 MPa were found at 0° and 90°, respectively.

Therefore, the focus of the present paper is conferring the peculiar properties for 3D printing extrusion to the material recycled from the disposable face masks. Different percentages of talc were added to the filtering material of pristine masks in a small scale equipment (production of a few tens of grams). Thus, considering the data obtained from rheological and thermal characterizations, two specific formulations were scaled up in a lab twin-screw extruder (production of a few hundred grams), by using pristine masks or recycling sanitized after use masks and first use PP copolymer. Finally, the pellets were spun and validated as material for 3D printing in commercial extrusion equipment. The quality of the 3D printed objects was evaluated through the microstructure observations and the comparison of the mechanical properties of the 3D printed standard tensile specimens with a commercial 3D printable material.

## 2. Materials and methods

The small-scale preliminary study consisting in adding talc to the pristine masks was carried out using a mini-extruder with a recirculation channel as experienced in previous studies [19] (Figure S1) with parameters specified in the section 2.2.1. The materials in the quantity of a few grams were characterised for rheological and thermal behaviours to evaluate the suitability for 3D printing, as detailed in 2.3 section.

The scale-up of the process was assessed with a lab scale twin-screw extruder with a continuous extrusion line composed of feeding units, extruder, cooling tank and pelletizing system (Figure S2 parameters specified in the section 2.2.2). The resulting materials were used for filament fabrication and 3D printing following the guidelines described in the article by Bertolino et al. [23] regarding pristine PP material and parameters specified in section 2.2.2.

## 2.1. Materials

The pristine disposable face masks were purchased from Xiantao Wenjun non-woven co., Ltd. (China). The deep characterization of such kind of masks is presented in a previous article [19].

The after use masks (unknown brand) were collected in dedicated bins in schools and some local companies for few weeks and brought sealed by volunteers to Greenlife multiservices s.r.l. for the sanitization with ozone generated with Ozonplus equipment. The ozone is flowed into a chamber containing the masks and left to act for some minutes. The sanitized masks were then delivered in sealed bags without any further treatment.

For both kind of masks, the facial filtering parts were coded as M for pristine and AUM for after use masks after a manual separation of the metal nose clips and the ear loops.

A polypropylene-polyethylene copolymer "ISPLEN PB 170 G2M" produced by Repsol-Chemicals (MFI=12, Density 905 g/cm$^3$, Flexural modulus 1200 MPa from supplier data sheet) was used as partial substitute of mask material and coded as PP following the 3D printable guidelines defined by Jin et al. [24].

Talc HTP1 grade produced by IMI FABI Spa ($D_{50}$=1.9 µm, $D_{98}$=8.0 µm; density 2.8 g/cm$^3$ and specific surface area (SSA) 10 m$^2$/g) was used as filler in the compounds and coded as T.

The polypropylene filament “P-LENE T15” by Treed Filaments was used as commercial reference for the realization of 3D printed standard tensile tests specimens.

## 2.2. Equipment and processes for production

### 2.2.1. Small scale approach

Pristine masks were hot pressed at 190°C for 3 minutes at 50 bar pressure in a mold of 10x10x0.3 cm$^3$ with Collin P 200 T machine and then granulated (diameter smaller than 5 mm) with a Piovan Rsp15/15 mill, in order to feed easily the co-rotating twin-screw mini-extruder Xplore MC 15 (15 cm$^3$).

Thus, the material was melt-mixed with talc in several percentages by means of a manually fed mini-extruder (details in Table 1). The screw speed was maintained at 50 rpm during feeding time and increased to 100 rpm for the 2 min of residence time. The heating temperature was selected at 190°C.

The materials thus obtained have been coded (Table 1) with numbers corresponding to the percentages and the acronym of the corresponding material: e.g. 70M30T is the material with 70 wt.% of pristine masks and 30 wt.% of talc.

*Table 1. Codes, compositions of the materials and equipment used for compounding.*

| Code | M [wt.%] | AUM [wt.%] | PP [wt.%] | T [wt.%] | Scale | Screw speed [rpm] | Total flow [g/h] |
|---|---|---|---|---|---|---|---|
| **100M** | 100 | - | - | - | Small | 100 | - |
| **90M10T** | 90 | - | - | 10 | Small | 100 | - |
| **80M20T** | 80 | - | - | 20 | Small | 100 | - |
| **70M30T** | 70 | - | - | 30 | Small | 100 | - |
| **60M40T** | 60 | - | - | 40 | Small | 100 | - |
| **35M35PP30T** | 35 | - | 35 | 30 | Lab | 200 | 350 |
| **50M20PP30T** | 50 | - | 20 | 30 | Lab | 100 | 175 |
| **35AUM35PP30T** | - | 35 | 35 | 30 | Lab | 200 | 350 |
| **50AUM20PP30T** | - | 50 | 20 | 30 | Lab | 100 | 175 |

### 2.2.2. Lab scale approach

The M and AUM were shredded directly with the Piovan Rsp15/15 mill to form little pieces of a fluffy material similar to raw cotton (Figure S3).

The material thus obtained was manually fed into the ThermoFisher Scientific twin-screw extruder (Process 11). The extrudate was cooled in a water-containing tank and pelletized with a rotating cutter (Varicut pelletizer 11 mm). This first extrusion step was necessary to produce granules of constant dimensions, able to load the volumetric feeder of the extruder in the second extrusion step. The M or AUM pellets thus obtained were manually mixed with PP and compounded with T to produce selected formulations with the same twin-screw extruder (details in Table 1). The screw speed varied from 100 to 200 rpm and the total flow from 175 to 350 g/h (details in Table 1). The heating temperature profile was set from 190°C (feeder) to 180°C (head). The screw profile adopted during all extrusions is shown in Figure 1. Each element is identified with an abbreviation describing the type.

Two volumetric feeders (MT and RT model from Brabender) were used: the first supplies the polymer and is located at the begin of the extruder; the second, for the talc powder, is placed about halfway through the barrel (Figure 1).

A vent-port at atmospheric pressure is located at the end of the extruder barrel (Figure 1) in order to have a compound free of residual volatiles.

The materials thus obtained have been coded with numbers corresponding to the percentages and the acronym of the corresponding material (Table 1): e.g. 35M35PP30T is the material with 35 wt.% of pristine masks, 35 wt.% of PP copolymer and 30 wt.% of talc.

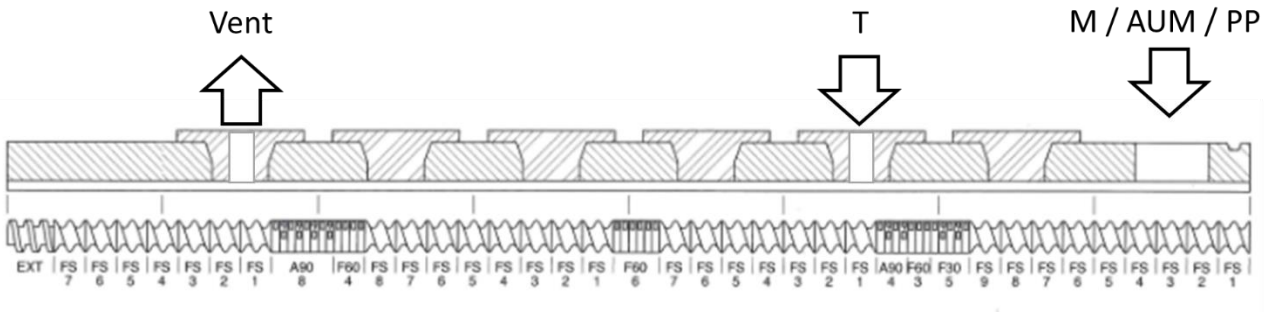


*Figure 1. Screw profile (FS = conveying element. F30, F60, A90 = kneeding elements, promote both distributive and dispersive mixing. The number indicates the phase shift angle between the lobes of the element. EXT = exit element, facilitates the release of the melt from the extruder.)*

Next 1.0 Advanced filament making machine by 3Devo has been used to produce a filament with a nominal diameter of 1.75 mm. This machine is composed of a single-screw extruder, an air cooling system, two rollers that pull the extruded material and a filament rolling system on a spool. The speed of the rollers is controlled by an automatic system that adjust it in order to maintain the filament diameter set value. The detailed procedure used is the same as described in a previous article [23]. The process parameters optimized for all the formulations are: heating temperatures between 175 °C (feeder) and 190 °C (die), screw speed set at 3.5 rpm and working percentage of the cooling fans to 40%.

Roboze One 3D printer equipped with a 0.4 mm nozzle was used to prepare tensile test specimens (ISO 527 standard type 5A) with the help of Simplify 3D software. The 3D printer bed was fully covered with a PP surface to enhance the 3D printing adhesion. An extrusion speed of 30 mm/s, 100% of infill percentage, ±45° as the deposition pattern, 0.4 mm for the extrusion width, 0.2 mm for the layer thickness, 70% of outline overlap and 50°C for the bed temperature were used. The profile of extrusion temperatures from 190 to 240°C, as detailed in the experimental section, was adopted.

Thirteen layers were deposited: three layers for the raft and ten layers for the tensile specimen with two perimeter shells.

## 2.3. Characterization techniques

Thermal properties were evaluated with Differential Scanning Calorimetry (DSC) and Thermogravimetric Analysis (TGA) on the compounded pellets.

The DSC equipment was a Q20 by TA Instruments, requiring samples of 8 ± 1 mg. The chamber was purged with 50 mL/min nitrogen. Each sample was heated from -50°C to 220°C at 10°C/min twice, in order to firstly erase the previous thermal history. The Crystallization temperature (Tc) was assumed as the abscissa of the heat flow main peak during the cooling cycle and the Crystallization Enthalpy (ΔHc) was evaluated as the integral of the same peak.

The equipment used for TGA is a Discovery thermo balance by TA Instruments. The samples of approximately 10 mg were placed in open alumina pans. The analyses were carried out in fluxed air (25 mL/min), from 50 to 700 °C with a heating rate of 10 °C/min.

Rheological properties were evaluated using a TA Instrument ARES strain-controlled parallel plate geometry rheometer (plate diameter: 25 mm). Preliminary strain sweep tests were carried out at ω = 100 rad/s and 230 °C. The complex viscosity, storage and loss moduli were measured during the frequency scans from $10^2$ to $10^{-1}$ rad/s at 230°C. The strain amplitude was selected for each sample in order to fall in the linear viscoelastic region.

The samples for rheological analyses were shaped using a hot plates press Collin P 200 T. The 25 mm diameter and 1 mm thickness disks were obtained by pressing for 3 minutes the pellets at 50 bar into a metallic mould heated at 190°C.

A modified Carreau equation [33] was used to fit the experimental complex viscosity curves:

$$\eta^*(\omega) = \frac{\eta_0}{[1+(\lambda\omega)]^{(1-n)}} + \frac{\sigma_0}{\omega} \qquad \text{Eq.(1)}$$

Where $\sigma_0$ is the melt yield stress, $\eta_0$ is the zero shear viscosity, $\lambda$ is the relaxation time and $n$ is the dimensionless power law index.

Tensile tests were performed following ISO 527 standard at room temperature with an Instrom 5966 machine equipped with 2 kN pneumatic grips. Using a loading cell of 2 kN (error <0.25%), the measurement parameters were an initial strain rate of 1 mm/min that increased up to 10 mm/min once a deformation of 0.25% was exceeded. The samples had gauge length of 50 mm and the deformation was calculated by a position transducer. Six specimens were used for each formulation and the

average values and corresponding standard deviations of the tensile modulus (E), elongation at break (ε) and maximum tensile strength (σ) were calculated and reported.

The surface morphology and section of filaments were investigated using an EVO 15 Scanning Electron Microscope (SEM) from Zeiss (beam voltage: 20 kV working distance: 8.5 mm). The surfaces were directly investigated by cutting small pieces and covering with a sputtered gold layer.
The real time diameter of the filament was measured and recorded during the extrusion with DevoVision software, developed by 3Devo. The average and standard deviation of the filament diameter were calculated from the data recorded.
The filling percentage of 3D printed object as the percentage deviation from the theoretically full filled item was evaluated using the formula:

$$Filling\ percentage\ [\%] = \left(\frac{Average\ weight\ specimen}{Volume\ specimen * Filament\ density} - 1\right) \times 100 \qquad \text{Eq.(2)}$$

Where the Average weight was directly measured from the 3D printed objects after the removal of the raft part and the theoretical weight of full filled object was calculated from the actual volume of the specimen multiplied by the density of the filament determined by Archimedes' law (following ISO 1183 on pieces of about 5 centimetres in length).
All dimensional measurements of the printed specimens necessary for the volume calculation were made using a digital caliper (Mitutoyo Corp CD-15CPX) with an accuracy of 0.01mm.

# 3. Results and discussion

## 3.1. Evaluation of the material properties for 3D printing extrusion purposes

### 3.1.1. Talc (T) addition to the mask material (M)

In the first place, it was investigated the effectiveness of talc as a shrinkage minimizer during melt solidification of M material. Generally, by adding a small amount of talc (1-2 wt.%) the polymer crystallisation is promoted. This is due to the fact that introducing a second phase in a polymer leads to heterogeneous nucleation of polymer crystalline domains [34]. On the other hand, inorganic fillers used at relatively high quantity (>10 wt.%) are well known to increase the dimensional stability of moulded parts [35-37]. Therefore, the shrinkage of the material could be reduced by adding the inorganic filler. For this reason, the crystallization enthalpy (ΔHc) of the materials were considered. The lower is this value, the smaller is the crystalline part formed during cooling, the lower the volumetric shrinkage. Taking the enthalpy of 100M as reference, the reduction percentage for the various formulations was calculated. As can be seen from the data shown in Table 2 (plot data

reported in Figure S4), as the talc content increases there is an increase in this percentage. Thus, confirming the quantity of talc introduced decreases the shrinkage of the material.
The data reported in Table 2 as residue from the TGA test is mainly used to verify the exact concentration of talc in the samples, which is confirmed to be close to the nominal value. Complete plot of the TGA data are available in the supporting information (Figure S5).

*Table 2. Characteristic data obtained from DSC and TGA analyses of M-T based formulations (ΔHc ref. is the 100M formulation).*

| **Code** | **Tc [°C]** | **ΔHc [J/g]** | **(ΔHc - ΔHc ref.) / ΔHc ref. [%]** | **Residue at 700°C [%]** |
|---|---|---|---|---|
| **100M** | 119 | 99.5 | ref. | 0.5 |
| **90M10T** | 124 | 92.9 | -7 | 10.2 |
| **80M20T** | 125 | 73.6 | -26 | 20.8 |
| **70M30T** | 126 | 72.2 | -27 | 29.7 |
| **60M40T** | 126 | 64.9 | -35 | 38.4 |

In a previous work [23] a PP-based material for 3D extrusion purpose containing 20 wt.% of talc presented a melting enthalpy of 74 J/g, substantially comparable to that found in this paper. The material from the mask behaves thus similarly to a commercial material considering the introduction of the same amount of talc.

Generally, the introduction of talc particles modifies also the rheological behaviour of polymers, erasing the Newtonian plateau present at low frequencies and providing a yield stress. This performance is particularly recommended for 3D printing material extrusion, because it allows the material to be stable when deposited [38, 39]. On the other hand, the addition of a filler can also be used to increase the viscosity of the 100M material which has proved to be very low [19]. Such improvement is mandatory for some applications, for example for 3D printing process, as reported in the literature [23, 39].

The complex viscosity curves of the compounded materials as a function of the frequency have been fitted using a modified Carreau model (Eq. 1) [33]. In Figure 2 the curves are reproduced and in Table 3 the fitting parameters are reported.

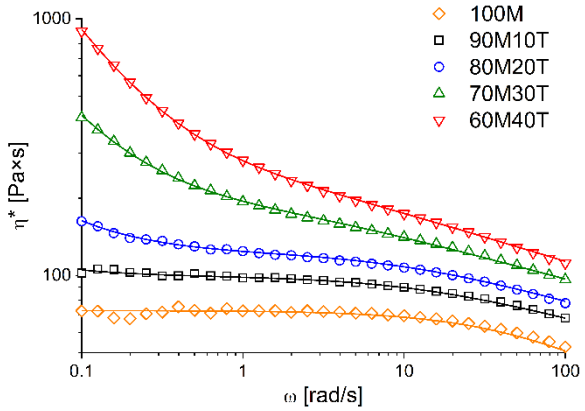


*Figure 2. Rheological experimental point obtained at 230°C for M-T based formulations and fitting curves with modified Carreau model.*

*Table 3. Specifications of the modified Carreau model parameters used for fitting the rheological curves of M-T formulations obtained at 230°C.*

| | $\eta_0$ [Pa×s] | $\lambda$ [1/s] | n | $\sigma_0$ [Pa] | $R^2$ |
|---|---|---|---|---|---|
| **100M** | 73 | 0.02 | 0.67 | 0.0 | 0.9334 |
| **90M10T** | 99 | 0.08 | 0.83 | 0.6 | 0.9893 |
| **80M20T** | 122 | 0.10 | 0.82 | 4.2 | 0.9981 |
| **70M30T** | 180 | 0.38 | 0.83 | 24.2 | 0.9992 |
| **60M40T** | 224 | 0.36 | 0.81 | 68.6 | 0.9998 |

From the data reported in Table 3, it can be seen that both $\eta_0$ and $\sigma_0$ increase as a function of the talc amount. Specifically, the sample with 40 wt.% of talc rises to an appreciable $\sigma_0$ value of 68.6 Pa.

Comparing the results obtained with those designed for 3D printing purposes presented in a previous work (namely, PP COPO + 20% TALC in ref. [23]), the zero shear viscosity ($\eta_0$) is one order of magnitude lower for all the formulations ($10^2$ vs. $10^3$ Pa.s). As well as the yield stress ($\sigma_0$) was concerned, all the formulations do not reach the value of 115 Pa at 230°C [23].

Thanks to these comparisons, it can be concluded that the type of polypropylene deriving from the masks and the quantity of talc added are therefore inadequate to increase both the $\eta_0$ and $\sigma_0$. Following the progressive trend reported for the formulations ranging from 10 to 40 wt.% of T, probably a greater filler addition could bring to the desired rheological behavior. On the other hand, generally a material with a high filler loading is fragile and a continuous filament very complicated to obtain during the extrusion process, thus inappropriate for 3D printing purposes [37, 38]. For this reason, the strategy of adding first use PP to the material was pursued.

### 3.1.2. Trial formulations of pristine masks (M), first use copolymer (PP) and talc (T)

A PP copolymer was selected, in accordance with the study of Bertolino et al. [23], which highlighted the better yield stress and lower enthalpy resulting in the addition of a certain amount of talc, if compared to the Polypropylene homopolymer and the research of Jin et al. on PP grade for 3D printing [24].

The first formulation involves the replacement of 50% of the masks material with PP while the second one only ca. 30%. As can be observed in Table 4 (plot data in Figure S6), both formulations show a lower value of crystallization enthalpy than the neat masks (72.2 J/g used as reference ΔHc ref. in Table 2), the copolymer is therefore able to reduce enthalpy also mixed to the M material due to its lower crystallinity (79.5 J/g, plot data in Figure S7). Using a greater quantity of PP (35%) results in a lower enthalpy value (-15% with respect to 70M30T sample). The residue from TGA analyses (plot data in Figure S8) confirms that the formulations contain an amount of talc (around 31.5%) close to the desired nominal value.

*Table 4. Characteristic data obtained from DSC and TGA analyses of M-PP-T and AUM-PP-T formulations (ΔHc ref. is the ΔHc of 70M30T formulation).*

| Code | Tc [°C] | ΔHc [J/g] | (ΔHc - ΔHc ref.) / ΔHc ref. [%] | Residue at 700°C [%] |
|---|---|---|---|---|
| **70M30T** | 126 | 72.2 | Ref. | 29.7 |
| **35M35PP30T** | 127 | 61.6 | -15 | 31.6 |
| **50M20PP30T** | 126 | 66.2 | -8 | 31.5 |
| **35AUM35PP30T** | 127 | 57.1 | -21 | 36.8 |
| **50AUM20PP30T** | 126 | 64.5 | -11 | 30.2 |

In addition, rheological tests were also carried out (Table 5). Considering the complex viscosity, the two formulations have values significantly higher than the formulation with the same amount of talc and M, 70M30T (3260 and 3853 vs. 180 Pa·s). On the other hand, considering the yield stress $\boldsymbol{\sigma_0}$, the greater M presence in the formulation decreases the value from 1650 to 1238 Pa. At the same time, both data are still considerably higher than what was found in the M-T system best formulation (60M40T: 69 Pa).

*Table 5. Specifications of the modified Carreau model parameters used for fitting the rheological curves of M-PP-T and AUM-PP-T formulations obtained at 230°C.*

| | $\boldsymbol{\eta_0}$ **[Pa×s]** | $\boldsymbol{\lambda}$ **[1/s]** | **n** | $\boldsymbol{\sigma_0}$ **[Pa]** | $\mathbf{R^2}$ |
|---|---|---|---|---|---|
| **35M35PP30T** | 3260 | 0.97 | 0.58 | 1650 | 0.9989 |
| **50M20PP30T** | 3853 | 3.87 | 0.60 | 1238 | 0.9998 |
| **35AUM35PP30T** | 594 | 0.11 | 0.26 | 2371 | 0.9861 |
| **50AUM20PP30T** | 233 | 0.04 | 0.34 | 995 | 0.9511 |

At the end of this trial on pristine face masks, the two formulations presented are validated for the 3D printing.

### 3.1.3. Trial formulations of after use masks (AUM), first use copolymer (PP) and talc (T)

Once the selected formulations proved to be suitable for 3D printing, they have been produced replacing M with AUM. In this case, the masks were obtained from on-site harvesting in schools, therefore the brand is unknown. This step was chosen to get as close as possible to the potential industrial recycling, where several batches with different origins will be mixed and the after use collecting can make changes in the purity of the materials. On the other hand, the collection bins were dedicated to surgical masks only, thus limiting the possible heterogeneity of the materials.

The production process is detailed in the materials and methods section and a visual representation is presented in the Figure S2.

The enthalpies measured for AUM-PP-Ts are even lower than that of the corresponding M-PP-Ts (57.1 vs. 61.6 and 64.5 vs. 66.2, Table 4) and maintain the same trend with respect to the neat masks 70M30T (-21% and -11%, respectively).

No other crystallization peaks are present in the DSC plot (Figure S6) excepting the one already identified for PP. Also, no other degradation processes emerged from the TGA analyses (Figure S8) other than that attributed to PP. Thus, the material deriving from post-use recycling do not present substantial differences compared to the material deriving from pristine masks.

The TGA residue shows that the actual quantity of talc in 35AUM35PP30T is not as close to the desired 30 wt.%. Concentration variations may have occurred during extrusion due to low extrusion speed and non-homogeneous size of PP and AUM pellets.

Comparing the rheological properties of AUM-PP-Ts and M-PP-Ts (*Figure* 3 and Table 5), the calculated zero shear viscosity ($\eta_0$) and the yield stress ($\boldsymbol{\sigma_0}$) are extrapolated. The experimental data of AUM-PP-T materials at low shear stresses cross and exceed the values of corresponding M-PP-T (*Figure* 3), that is the evidence of a higher yield stress. This can be appreciated from the experimental plot in Figure 3 with respect to the fitting parameters in Table 5. Indeed, the intense deviation (low $R^2$ value in Table 5) between fitting curves and experimental points in this part of the curve does not allow an accurate evaluation through the fitting.

On the other hand, the variation in the rheological properties between M-PP-Ts and AUM-PP-Ts is undoubtedly clear and is due to the diversified origin of the masks along with the presence of "dirt" collected during their use.

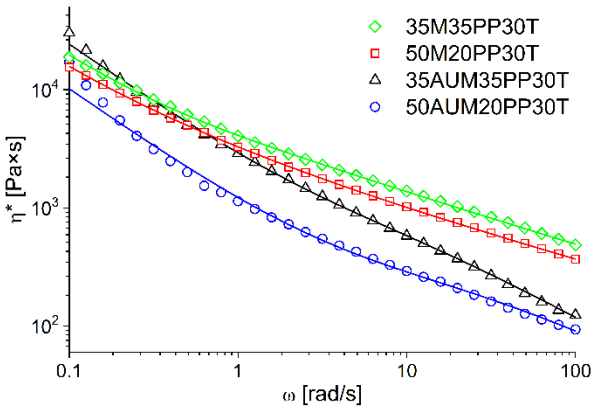


*Figure 3. Rheological experimental point obtained at 230°C for M-PP-Ts and AUM-PP-Ts and fitting curves with modified Carreau model.*

## 3.2. AUM-based materials: filament making process and analysis

From the results reported in the previous section, the two AUM-based materials were found potentially 3D printable. With these formulations, the production of the filaments for 3D printing was then carried out.

The filaments were extruded with Next 1.0 Advanced machine optimizing the process parameters.

The filament quality was evaluated by observing directly surface roughness and geometry using SEM (Figure 4).

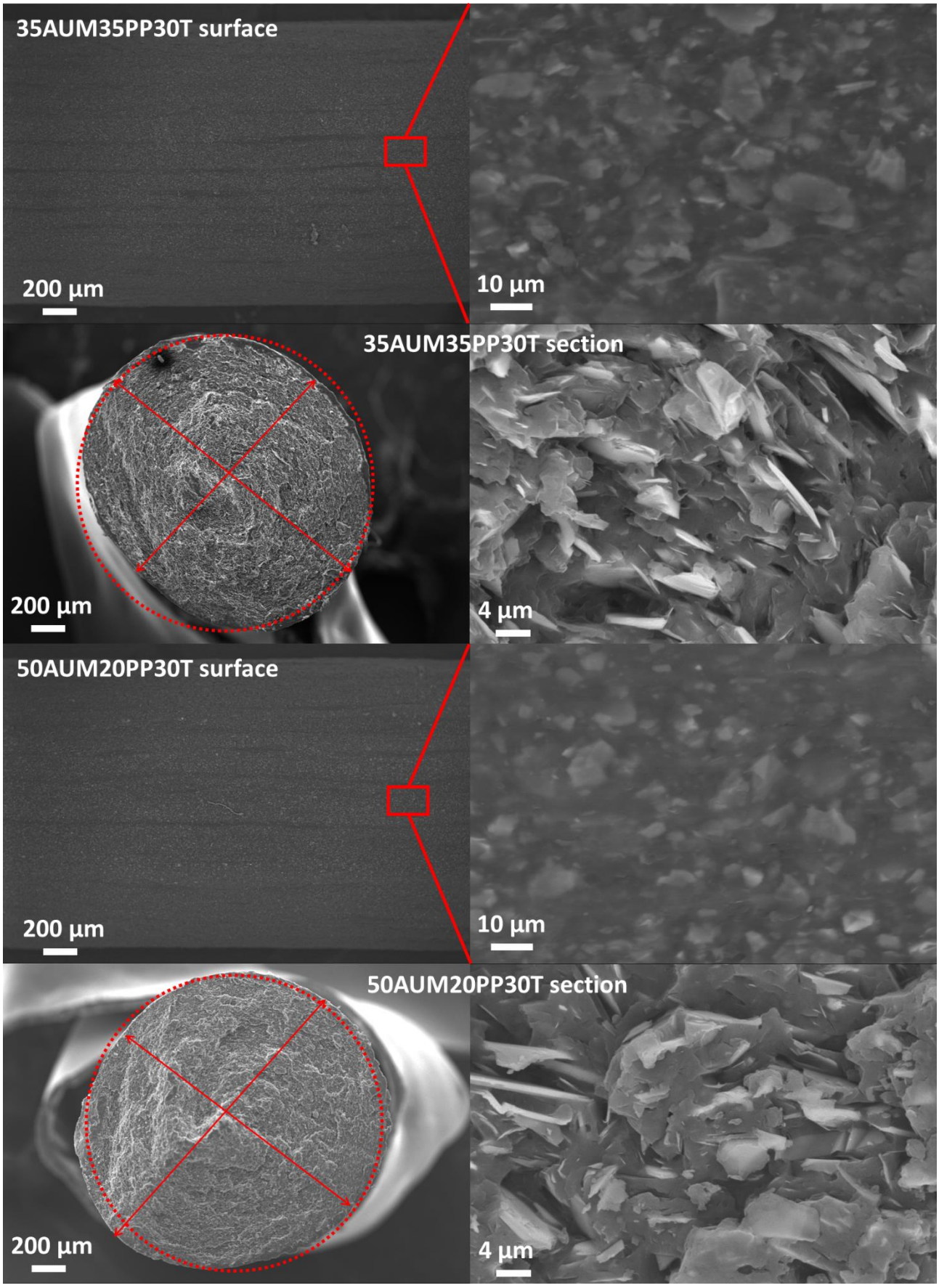


*Figure 4. SEM images of the surface and section of 35AUM35PP30T and 50AUM20PP30T filaments.*

As far as roughness was concerned, the surface of both formulations presents horizontal signs as wrinkles that make it difficult to make an in-depth visual comparison. However, higher magnifications on the surfaces reveal the presence of well distributed and dispersed talc lamellae in the matrix. In addition, in Figure 4 the magnifications of the cross-sections highlight the uniform dispersion of the talc in throughout the matrix and the preferential orientation in the direction of the extrusion (out of plane in the images).

Referring to the geometry, the oval cross-sections is highlighted in Figure 4 by superimposing a circumference to the major and minor axes of the filaments. The values measured with SEM correspond to 1.83 and 1.56 mm for 35AUM35PP30T and 1.87 and 1.69 mm for 50AUM20PP30T. The average diameters calculated with DevoVision software are respectively 1.76 ± 0.15 mm and 1.54 ± 0.09 mm. Thus, compared to the nominal 1.75 mm value, 35AUM35PP30T filament shows a more accurate and less precise diameter, meanwhile for 50AUM20PP30T filament a more precise and less accurate value turns out (Figure S9).

These results are in accordance with Pan et al. [31], that produced filaments having diameters within 1.67–1.78 mm, with less than 6% of tolerance.

## 3.3. 3D printing optimisation and characterization

As for the filament making, parameters optimisation also affected the 3D printing process focussing mainly on extrusion temperatures. The other parameters have been kept constant: 100% of infill percentage, ±45° as the deposition pattern, 0.4 mm for the extrusion width, 0.2 mm for the layer thickness, 30 mm/s as the extrusion speed and 50°C as bed temperature.

Both 35AUM35PP30T and 50AUM20PP30T required a temperature ramp (Figure 5). Temperatures are named as follows. TL1 is the raft production temperature (layer 1, 2, 3). TL4 refers to the first layer of the sample, set in order to facilitate removal from the raft. TL5 and TL11 are the temperatures of the core and the upper part of the specimen, set up to improve the adhesion of the two external perimeters and to avoid their separation from the inner part.

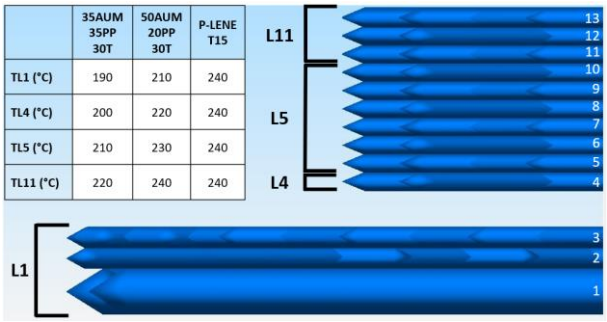


*Figure 5. 3D printing slicing design for raft (layers 1-3) and part (layers 4-13) and corresponding temperatures used.*

35AUM35PP30T requires higher printing temperatures than 50AUM20PP30T because, due to the lower content of mask and the higher content of PP, the filament accumulates inside the nozzle stopping the printing process. P-LENE T15 instead was printed at the constant temperature of 240 °C as reported in the manufacturer's data sheet.

Therefore, it was verified that the two formulations are suitable for 3D printing, even if greater care in the process parameters setting is required.

Table 6 and Figure 6 report some qualitative and quantitative evaluations on the 3D printed objects.

*Table 6. Final quality evaluated in terms of dimensions (L=length W=width T=thickness), calculated volume, filament density and filling percentage.*

| Code | Dimensions [mm] | Volume [$cm^3$] | Filament Density [$g/cm^3$] | Filling percentage [%] |
|---|---|---|---|---|
| | L=75.28±0.22 | | 1.20 | -20 |
| **35AUM35PP30T** | W=4.22±0.16 | | | |
| | T=2.44±0.23 | 1.62 | | |
| | L=74.73±0.28 | | 1.14 | -25 |
| **50AUM20PP30T** | W=4.09±0.18 | | | |
| | T=2.30±0.13 | 1.47 | | |
| | L=75.25±0.21 | | 1.00 | -20 |
| **P-LENE T15** | W=4.29±0.02 | | | |
| | T=2.44±0.04 | 1.64 | | |

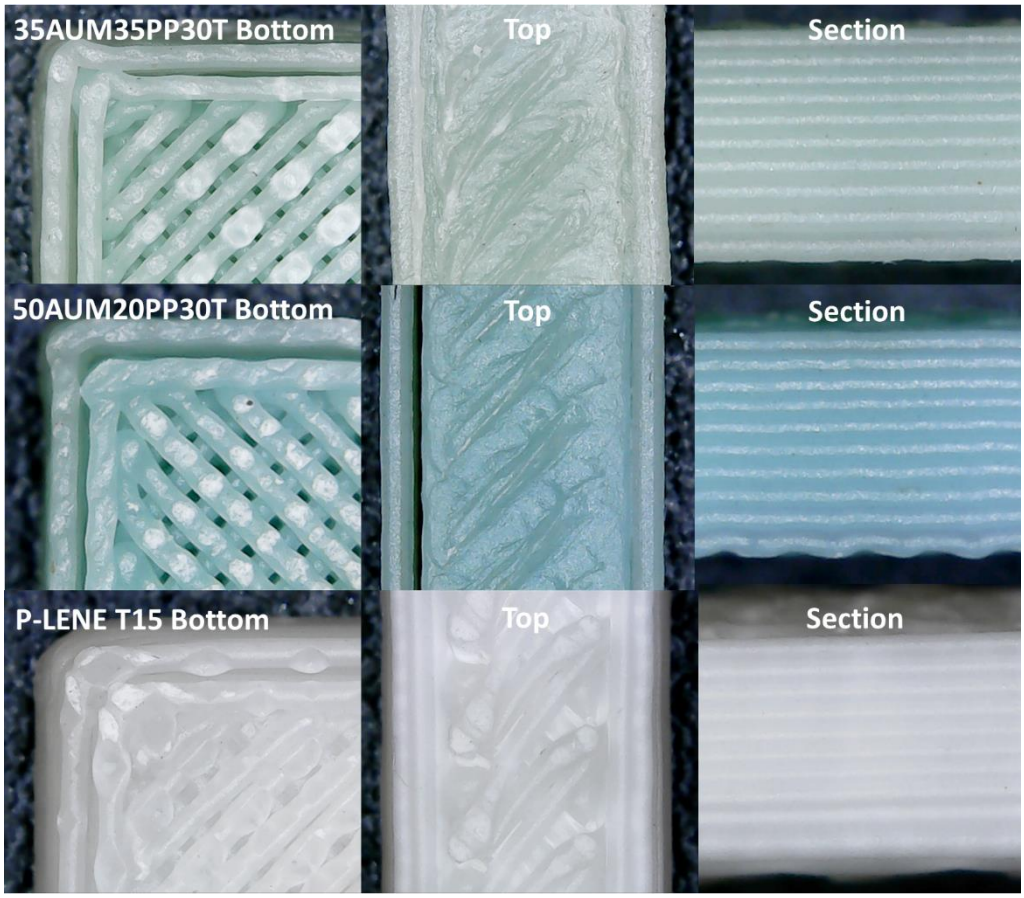


*Figure 6. Final quality of 3D printed specimens evaluated in terms of: definition of details in the bottom and top orientation, check of the occurrence of adhesion problems between the layers in the perimeter and sections.*

The quality assessment considered the compliance with the nominal dimensions, the filling percentage of the printed objects, the definition of details, the occurrence of problems in layer adhesion between the sample and the raft or the printing plate.

The nominal dimensions of the 3D printed object are: 75 mm for the length, 4 mm for the width and 2 mm for the thickness of the reduced section and 1.25 $cm^3$ of volume. All materials have mean values of width and thickness greater than the nominal value (see W and T data in Table 6) with the greatest deviation for thickness (35AUM35PP30T and P-LENE T15 +22%, while 50AUM20PP30T +15%). The width is more accurate and presents a deviation from the nominal value of 6%, 2% and 7% for 35AUM35PP30T, 50AUM20PP30T and P-LENE T15. The length is generally the most accurate dimension and, in the case of the 50AUM20PP30T, it is even shorter. From these measurements, the volume of the samples and the filling percentage (according to Eq. 2) were calculated and reported in Table 6.

The filling percentage of the various samples turned out to be always negative, thus the objects are less fill than they should be. The 35AUM35PP30T and P-LENE T15 have -20% of filling percentage, whereas 50AUM20PP30T led to a value of -25%.

Considering both the dimensions of the object and the filling, 50AUM20PP30T show dimensions closer to the nominal values and lower filling percentage. This may be due to the lowest filament average diameter, which therefore leads to the worse filling during the 3D printing process. In the other two cases the size of the objects is significantly greater than the nominal one but the filling percentage is always lower than the theoretical expected. The printing conditions adopted and the 3D printer in use therefore do not allow to reach the optimal filling even with a commercial filament.

In Figure 6 are highlighted the aesthetic differences among the samples. The magnifications are obtained with an optical microscope on one of the specimens for the mechanical tests. All samples were viewed from the side detached from the raft (coded as bottom), on the opposite side (coded as top) and sideways (coded as section). Both the 35AUM35PP30T and the 50AUM20PP30T show the separation of the perimeter at the bottom, while the P-LENE T15 has a much more compact morphology. Looking at the samples from the top, the surfaces of the 35AUM35PP30T and the P-LENE T15 are compact; instead, 50AUM20PP30T presents a short separation stretch between the perimeter and the inner part of the specimen. Moreover, the first layers of 35AUM35PP30T and 50AUM20PP30T present a general undulation, while for P-LENE T15 a more linear structure is reported. A further qualitative indication of sample section filling is presented in Figure S10 in the supporting information.

The final comment on the quality of 3D printed objects can be summed up with a better quality of the reference material with respect to the sample with mask material, but its filling percentage is completely comparable to the 35AUM35PP30T solution. In order to have other useful information for the qualitative evaluation of 3D printed materials, the mechanical properties are presented.

## 3.4. Mechanical properties

The mechanical properties of the mask-based and reference materials were measured on the 3D printed samples. The tensile modulus (E), maximum tensile stress ($\sigma$) and elongation at break ($\varepsilon$) were reported in Figure 7.

The elastic moduli of 35AUM35PP30T and 50AUM20PP30T resulted 1.38 and 1.25 GPa, respectively. The neat PP of the pristine masks gave a modulus of 825 MPa on a compression moulded

specimen [19]. In this case, the material was not talc filled and therefore the lower modulus is predictable.

These finding are consistent with the best modulus obtained from 3D printed specimens of recycled PP tested at 0° by Morales et al. [32] of 1.34 GPa. These data show how the formulation from recycled masks has a stiffness characteristic of other rPP and also similar to the PP copolymer present in the formulation (flexural modulus of 1.20 GPa from producer data sheet). Although the manufacturer of the commercial 3D filament P-LENE T15 declares a tensile stiffness of 1.95 GPa, the 3D printed samples show a modulus of 0.75 GPa, much lower than the two formulations containing masks.

Taking into consideration the maximum stress, the AUM-based materials are fully comparable to the commercial one (14-15 MPa for all the samples, see Figure 7). This result is very interesting as it certifies that the 3D printed objects with the materials deriving from the masks will be able to undergo the same stresses as the commercial material before breaking and deform less as its rigidity is greater.

Morales et al. [32] found different strengths results for PP specimens produced at 0° and 90° orientations. In the first case, the $\sigma$ of 26 MPa was reported, while for the second one, about 4 MPa. The samples produced in the present article are oriented at ±45°, therefore an intermediate value of strength is certainly plausible. Moreover, Zander et al. found a slightly higher strength value of 20.1 ± 2.3 MPa for neat rPP, confirming the eligibility of the research here presented for the final 3D application [27].

The neat PP from pristine masks reached a stress of 22 MPa [19]. On the other hand, a stress of about 16-17 MPa can be expected for the 3D printed formulations, when considering the possible pollution of the after use material and the fact that the samples are filled only for 75-80 % of the volume. Indeed, the values obtained are in accordance with the expectations.

On the other hand, the elongation at break is the most striking difference between the mask-based materials (2-3% of deformation) and P-LENE T15 (52%). The lower values for the AUM-based materials are due to the presence of talc and contaminants, in accordance with the research of Morales, that reports a deformations between 6% and 1% for recycled PP [32].

When considering deformation, is important to note that perimeter detaching from the core material could have led to a greater deformability only for P-LENE T15 (as visible in Figure 7). Concluding, the low deformability is a data to consider but it is not so demanding for 3D printing as generally the objects do not have to undergo large loads or deformations. The neat PP from pristine masks has an

elongation at break of 7% [19]. Thus, the formulations obtained mainly from this recycled material is expected to have a low elongation, even considering the presence of the filler.

Furthermore, there is no direct correlation between the production quality of the samples reported in section 3.3 and the mechanical properties here summarized. The 50AUM20PP30T sample was morphologically worse than the 35AUM35PP30T, but its mechanical properties are substantially comparable. This fact might suggest that if comparable filling percentage between the two were reached, the mechanical properties of 50AUM20PP30T would be even better.

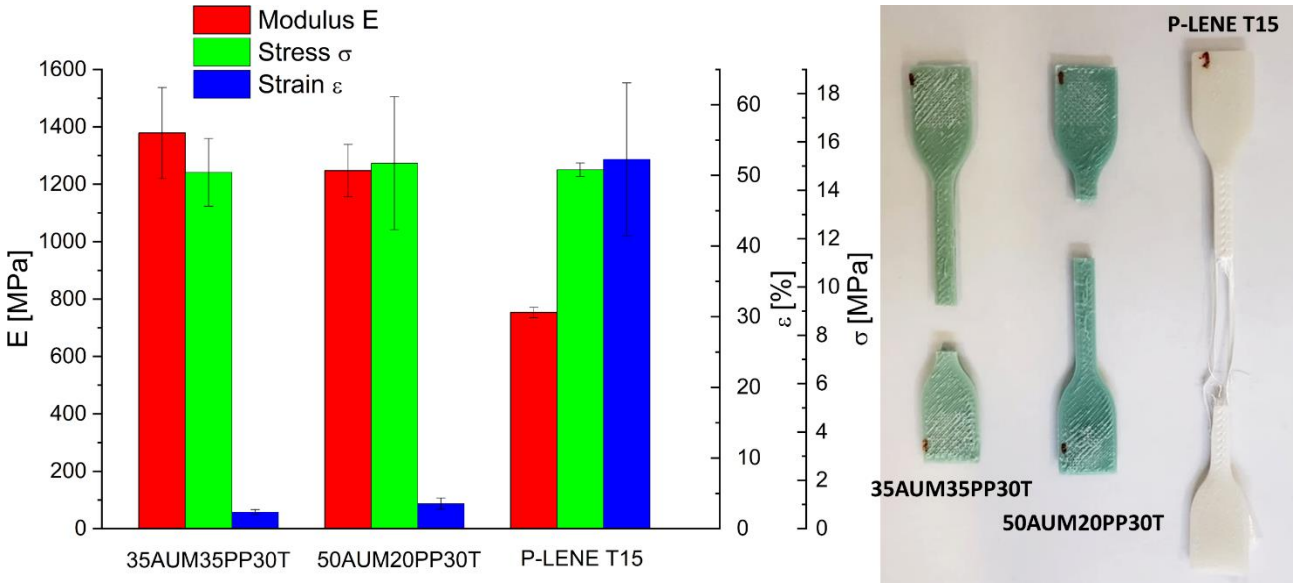


*Figure 7. Mechanical properties (tensile modulus (E), maximum tensile stress (σ) and elongation at break (ε)) of the AUM formulations and P-LENE T15 as well as a representative image of tensile specimens after break.*

The mechanical properties of 3D printed specimens have also been discussed by other authors, however data are not fully comparable because the filament instead of the specimen was tested. E.g. Pan et al. characterized the r-PE PP filament obtaining yield strength of 13.6 MPa and Young modulus of 1.23 GPa [31]. On the other hand, the filaments produced in this research were tested and the data followed the same trend detected on the 3D printed specimens even though presenting better tensile properties especially for the tensile strength (details in the supporting information Table S1).

It should be then emphasized that the mechanical properties as numerical value are not of crucial importance as it is unlikely that a 3D printed object will have mechanical resistance prerogatives. Moreover, different commercial filament based on PP could give drastically different mechanical properties. Thus, the most important result is that objects obtained with AUM have similar mechanical properties to a commercial PP-based 3D printed material.

# 4. Conclusions

The mask material recovery for 3D printing applications was proposed in order to recycle potentially harmful wastes, both as a source of micro plastic and consumption of resources impacting on the $CO_2$ production.

Based on the results in the present paper, it is not possible to have a material with rheological characteristics and volumetric shrinkage suitable for 3D printing directly from the mechanically recycled masks. Neither the mask-based materials with the addition of talc up to 40 wt.% is enough, notwithstanding the improve of the selected performances.

To overcome this limitation, the quantity of masks in the formulation has been partially replaced with first-use polypropylene copolymer. Two formulations with 35 wt.% and 50 wt.% material from masks were produced with pristine (M) and sanitized after-use masks (AUM).

Considering the rheological and shrinkage characteristics, the resulting materials were found to be suitable for the 3D printing technique and a filament of 1.75 mm nominal diameter was successfully produced with AUM-based material.

The filament with 35 wt.% of AUM has a section variability of 9% and mean diameter value of 1.76 mm, while the filament with 50 wt.% of AUM has a variability of 6% and average diameter of 1.54 mm. These filaments lead to a filling percentage deviation between the specimens for mechanical tests and the full filled geometry of -20% and -25%, respectively.

For both formulations, the mechanical tests showed a stiffness almost double and a strength completely comparable to the commercial 3D printable material. The difference in the toughness can be mainly attributed to a difference in the quality and amount of filler in the commercial material, which is also underlined by a different physical behaviour of the perimeter upon breaking.

It can be concluded that both formulations based on AUM are eligible for industrial experimentation and even to hypothesize a higher content of masks.

The results reported in the present article are the first case in which suitable filaments for the production of extruded 3D printed objects have been formulated from disposable filtering masks. Such findings are intended to be the forerunner for future developments of new formulations to valorise a such highly impacting waste.

**Acknowledgments**

The authors would like to thank Mrs. Giuseppina Iacono and Dr. Dario Pezzini for SEM analysis and Federico Cascio Ingurgio for the work during his master thesis and the supporting of the Mondovì municipality and Circolo delle Idee for the after use masks collection, sanitation and supply.

**Author Contributions**

Conceptualization (DB AF), Formal analysis (FC GB), Investigation (FC GB), Data curation (DB FC GB), Methodology (DB GB), Validation (DB), Visualization (DB FC GB), Writing – original draft (DB), Writing – review & editing (DB FC GB AF), Supervision (AF), Project administration (AF).

**References**

[1] I. Armentano, M. Barbanera, E. Carota, S. Crognale, M. Marconi, S. Rossi, G. Rubino, M. Scungio, J. Taborri, G. Calabro, Polymer Materials for Respiratory Protection: Processing, End Use, and Testing Methods, Acs Applied Polymer Materials 3(2) (2021) 531-548.

[2] M.H. Chua, W. Cheng, S.S. Goh, J. Kong, B. Li, J.Y.C. Lim, L. Mao, S. Wang, K. Xue, L. Yang, E. Ye, K. Zhang, W.C.D. Cheong, B.H. Tan, Z. Li, B.H. Tan, X.J. Loh, Face Masks in the New COVID-19 Normal: Materials, Testing, and Perspectives, Research (Wash D C) 2020 (2020) 7286735.

[3] K. O'Dowd, K.M. Nair, P. Forouzandeh, S. Mathew, J. Grant, R. Moran, J. Bartlett, J. Bird, S.C. Pillai, Face Masks and Respirators in the Fight against the COVID-19 Pandemic: A Review of Current Materials, Advances and Future Perspectives, Materials (Basel) 13(15) (2020).

[4] A.L. Allison, E. Ambrose-Dempster, D. T Aparsi, M. Bawn, M. Casas Arredondo, C. Chau, K. Chandler, D. Dobrijevic, H. Hailes, P. Lettieri, The environmental dangers of employing single-use face masks as part of a COVID-19 exit strategy, (2020).

[5] T.A. Aragaw, Surgical face masks as a potential source for microplastic pollution in the COVID-19 scenario, Mar Pollut Bull 159 (2020) 111517.

[6] N. Parashar, S. Hait, Plastics in the time of COVID-19 pandemic: Protector or polluter?, Sci Total Environ 759 (2021) 144274.

[7] J.C. Prata, A.L.P. Silva, A.C. Duarte, T. Rocha-Santos, Disposable over Reusable Face Masks: Public Safety or Environmental Disaster?, Environments 8(4) (2021) 31.

[8] J.C. Prata, A.L.P. Silva, T.R. Walker, A.C. Duarte, T. Rocha-Santos, COVID-19 Pandemic Repercussions on the Use and Management of Plastics, Environ Sci Technol 54(13) (2020) 7760-7765.

[9] S.W. Rhee, Management of used personal protective equipment and wastes related to COVID-19 in South Korea, Waste Manag Res 38(8) (2020) 820-824.

[10] K. Selvaranjan, S. Navaratnam, P. Rajeev, N. Ravintherakumaran, Environmental challenges induced by extensive use of face masks during COVID-19: A review and potential solutions, Environmental Challenges 3 (2021) 100039.

[11] N. Singh, Y. Tang, O.A. Ogunseitan, Environmentally Sustainable Management of Used Personal Protective Equipment, Environ Sci Technol 54(14) (2020) 8500-8502.

[12] S.S. Muthu, Y. Li, J.Y. Hu, P.Y. Mok, Quantification of environmental impact and ecological sustainability for textile fibres, Ecological Indicators 13(1) (2012) 66-74.

[13] B.W. Hartanto, D.S. Mayasari, Environmentally friendly non-medical mask: An attempt to reduce the environmental impact from used masks during COVID 19 pandemic, Sci Total Environ 760 (2021) 144143.

[14] D. Battegazzore, F. Cravero, A. Frache, Development of disposable filtering mask recycled materials: Impact of blending with recycled mixed polyolefin and their aging stability, Resources, Conservation and Recycling 177 (2022) 105974.

[15] J.C. Rubio-Romero, M. del Carmen Pardo-Ferreira, J.A.T. García, S. Calero-Castro, Disposable masks: Disinfection and sterilization for reuse, and non-certified manufacturing, in the face of shortages during the COVID-19 pandemic, Safety Science (2020) 104830.

[16] M.C. Celina, E. Martinez, M.A. Omana, A. Sanchez, D. Wiemann, M. Tezak, T.R. Dargaville, Extended use of face masks during the COVID-19 pandemic - Thermal conditioning and spray-on surface disinfection, Polym Degrad Stab 179 (2020) 109251.

[17] S. Bhattacharjee, P. Bahl, A.A. Chughtai, C.R. MacIntyre, Last-resort strategies during mask shortages: optimal design features of cloth masks and decontamination of disposable masks during the COVID-19 pandemic, BMJ Open Respir Res 7(1) (2020).

[18] L.F. Ludwig-Begall, C. Wielick, L. Dams, H. Nauwynck, P.F. Demeuldre, A. Napp, J. Laperre, E. Haubruge, E. Thiry, The use of germicidal ultraviolet light, vaporized hydrogen peroxide and dry

heat to decontaminate face masks and filtering respirators contaminated with a SARS-CoV-2 surrogate virus, J Hosp Infect 106(3) (2020) 577-584.

[19] D. Battegazzore, F. Cravero, A. Frache, Is it Possible to Mechanical Recycle the Materials of the Disposable Filtering Masks?, Polymers (Basel) 12(11) (2020) 2726.

[20] N. Narita, M. Sagisaka, A. Inaba, Life cycle inventory analysis of CO 2 emissions manufacturing commodity plastics in Japan, The International Journal of Life Cycle Assessment 7(5) (2002) 277-282.

[21] ISTAT, Popolazione per età, sesso e stato civile 2020, 2020. https://www.tuttitalia.it/statistiche/popolazione-eta-sesso-stato-civile-2020/. (Accessed 22-04-2121 2021).

[22] C. Crespo, G. Ibarz, C. Saenz, P. Gonzalez, S. Roche, Study of Recycling Potential of FFP2 Face Masks and Characterization of the Plastic Mix-Material Obtained. A Way of Reducing Waste in Times of Covid-19, Waste Biomass Valorization (2021) 1-10.

[23] M. Bertolino, D. Battegazzore, R. Arrigo, A. Frache, Designing 3D printable polypropylene: Material and process optimisation through rheology, Additive Manufacturing 40 (2021) 101944.

[24] M. Jin, C. Neuber, H.-W. Schmidt, Tailoring polypropylene for extrusion-based additive manufacturing, Additive Manufacturing 33 (2020) 101101.

[25] K. Mikula, D. Skrzypczak, G. Izydorczyk, J. Warchol, K. Moustakas, K. Chojnacka, A. Witek-Krowiak, 3D printing filament as a second life of waste plastics-a review, Environ Sci Pollut Res Int 28(10) (2021) 12321-12333.

[26] M.R. Khosravani, T. Reinicke, On the environmental impacts of 3D printing technology, Applied Materials Today 20 (2020) 100689.

[27] N.E. Zander, M. Gillan, Z. Burckhard, F. Gardea, Recycled polypropylene blends as novel 3D printing materials, Additive Manufacturing 25 (2019) 122-130.

[28] K. Pickering, D. Stoof, Sustainable Composite Fused Deposition Modelling Filament Using Post-Consumer Recycled Polypropylene, Journal of Composites Science 1(2) (2017) 17.

[29] N. Vidakis, M. Petousis, L. Tzounis, A. Maniadi, E. Velidakis, N. Mountakis, D. Papageorgiou, M. Liebscher, V. Mechtcherine, Sustainable Additive Manufacturing: Mechanical Response of Polypropylene over Multiple Recycling Processes, Sustainability 13(1) (2020) 159.

[30] M. Spoerk, F. Arbeiter, I. Raguz, C. Holzer, J. Gonzalez-Gutierrez, Mechanical Recyclability of Polypropylene Composites Produced by Material Extrusion-Based Additive Manufacturing, Polymers (Basel) 11(8) (2019).

[31] G.-T. Pan, S. Chong, H.-J. Tsai, W.-H. Lu, T.C.K. Yang, The Effects of Iron, Silicon, Chromium, and Aluminum Additions on the Physical and Mechanical Properties of Recycled 3D Printing Filaments, Advances in Polymer Technology 37(4) (2018) 1176-1184.

[32] M.A. Morales, A. Maranon, C. Hernandez, A. Porras, Development and Characterization of a 3D Printed Cocoa Bean Shell Filled Recycled Polypropylene for Sustainable Composites, Polymers (Basel) 13(18) (2021).

[33] G. Filippone, S. Carroccio, R. Mendichi, L. Gioiella, N.T. Dintcheva, C. Gambarotti, Time-resolved rheology as a tool to monitor the progress of polymer degradation in the melt state–Part I: Thermal and thermo-oxidative degradation of polyamide 11, Polymer 72 (2015) 134-141.

[34] L.A. Castillo, S.E. Barbosa, N.J. Capiati, Influence of talc genesis and particle surface on the crystallization kinetics of polypropylene/talc composites, Journal of applied polymer science 126(5) (2012) 1763-1772.

[35] K. Shelesh-Nezhad, A. Taghizadeh, Shrinkage behavior and mechanical performances of injection molded polypropylene/talc composites, Polymer Engineering & Science 47(12) (2007) 2124-2128.

[36] Y. Ryu, J.S. Sohn, B.C. Kweon, S.W. Cha, Shrinkage Optimization in Talc- and Glass-Fiber-Reinforced Polypropylene Composites, Materials 12(5) (2019) 746.

[37] D. Stoof, K. Pickering, Sustainable composite fused deposition modelling filament using recycled pre-consumer polypropylene, Composites Part B: Engineering 135 (2018) 110-118.

[38] C. Duty, C. Ajinjeru, V. Kishore, B. Compton, N. Hmeidat, X. Chen, P. Liu, A.A. Hassen, J. Lindahl, V. Kunc, What makes a material printable? A viscoelastic model for extrusion-based 3D printing of polymers, Journal of Manufacturing Processes 35 (2018) 526-537.

[39] R. Arrigo, A. Frache, FDM Printability of PLA Based-Materials: The Key Role of the Rheological Behavior, Polymers (Basel) 14(9) (2022).